Interplay of electron-phonon interaction and strong correlations: DMFT+Σ study

E. Z. Kuchinskii, I. A. Nekrasov, and M. V. Sadovskii
Institute of Electrophysics, Russian Academy of Sciences, Ural Division, 620016 Ekaterinburg, Russia
(Received 21 June 2009; revised manuscript received 21 August 2009; published 29 September 2009)

We perform investigation of the Hubbard model with interaction between strongly correlated conducting electrons on a lattice with Debye phonons. To solve the problem generalized dynamical mean-field DMFT +Σ method is employed with "external" self-energy Σ_{ph} corresponding to electron-phonon interaction. We present DMFT+Σ_{ph} results for densities of states and kinks in energy dispersions for a variety of model parameters, analyzing the interplay of recently discovered kinks of purely electronic nature and usual phonon kinks in the electronic spectrum.

DOI: 10.1103/PhysRevB.80.115124 PACS number(s): 63.20.kd, 71.10.Fd, 71.27.+a, 71.30.+h

I. INTRODUCTION

The problem of the interplay of strong electronic correlations with electron-phonon interaction is of central importance in the physics of highly correlated systems. Actually there is a rather long history of such studies, e.g., one of the most popular models for electron-phonon interaction (EPI) in strongly correlated systems is the so-called Hubbard-Holstein model (HHM). The Hubbard model[1] itself describes local Coulomb interaction of electrons on a lattice including, e.g., Mott-Hubbard metal-insulator transition. On the other hand the Holstein model contains local linear displacement-to-density interaction of conducting electrons with local (Einstein) phonon modes.[2]

Active investigations of the properties of the HHM were undertaken in the framework of dynamical mean-field theory (DMFT),[3] which is a nonperturbative approach with respect to interaction parameters of the Hubbard model. Among many others one should mention DMFT solution of HHM for the case where the impurity solver used was the numerical renormalization group (NRG) [for review of DMFT (NRG) applications see Ref. 4]. The mapping of HHM to Anderson-Holstein impurity was first performed by Hewson and Mayer.[5] It was shown that using NRG one can compute in a numerically exact manner total electron-phonon contribution to the self-energy of the problem, thus making solution of the HHM nonperturbative also with respect to electron-phonon coupling strength. One should note that the self-consistent set of DMFT equations is preserved in this approach.

However, up to now there are apparently no studies of strongly correlated electrons interacting with Debye phonons. It is even more surprising in view of the widely discussed physics of kinks in electronic dispersion observed in ARPES experiments 40–70 meV below the Fermi level of high-temperature superconductors,[6] which are often attributed to EPI.[7] To our knowledge the problem of kink formation on electronic dispersion caused by EPI in strongly correlated systems was briefly discussed within HHM in papers by Hague[8] and Koller *et al.*[9]

In this paper we report DMFT+Σ results for the Hubbard model supplemented with Debye phonons, assuming the validity of Migdal theorem (adiabatic approximation). We consider the influence of Debye phonons on the weakly and strongly correlated electrons, studying electron dispersion and density of states (DOS), in particular close to Mott-Hubbard metal-insulator transition. We analyze in detail how EPI affects electronic dispersions in correlated metal and discuss the interplay of recently discovered kinks of purely electronic nature in electronic dispersion[10] and usual phonon kinks in the electronic spectra.

The paper is organized as follows. First we introduce in Sec. II DMFT+Σ approach to the model at hand. Then in Sec. III calculated results are presented and discussed. Summary and conclusions are given in Sec. IV.

II. DMFT+Σ COMPUTATIONAL DETAILS

The major assumption of our DMFT+Σ approach is that the lattice and time Fourier transform of the single-particle Green's function can be written as

$$G_{\mathbf{p}}(\varepsilon) = \frac{1}{\varepsilon + \mu - \varepsilon(\mathbf{p}) - \Sigma(\varepsilon) - \Sigma_{\mathbf{p}}(\varepsilon)}, \tag{1}$$

where $\varepsilon(\mathbf{p})$ is the bare electron dispersion, $\Sigma(\varepsilon)$ is the *local* self-energy of DMFT, while $\Sigma_{\mathbf{p}}(\varepsilon)$ is some "external" (in general case momentum dependent) self-energy. The advantage of our generalized approach is the additive form of the self-energy (neglect of interference) in Eq. (1).[11–13] It allows one to keep the set of self-consistent equations of standard DMFT.[3] However there are two distinctions. First, on each DMFT iteration we recalculate corresponding external self-energy $\Sigma_{\mathbf{p}}(\mu, \varepsilon, [\Sigma(\varepsilon)])$ within some (approximate) scheme, taking into account interactions, e.g., with collective modes (phonons, magnons, etc.) or some order-parameter fluctuations. Second, the local Green's function of effective impurity problem is defined as

$$G_{ii}(\varepsilon) = \frac{1}{N}\sum_{\mathbf{p}} \frac{1}{\varepsilon + \mu - \varepsilon(\mathbf{p}) - \Sigma(\varepsilon) - \Sigma_{\mathbf{p}}(\varepsilon)} \tag{2}$$

at each step of the standard DMFT procedure.

Eventually, we get the desired Green's function in the form of Eq. (1), where $\Sigma(\varepsilon)$ and $\Sigma_{\mathbf{p}}(\varepsilon)$ are those appearing at the end of our iteration procedure. To treat electron-phonon interaction for strongly correlated system we just introduce $\Sigma_{\mathbf{p}}(\varepsilon) = \Sigma_{ph}(\varepsilon, \mathbf{p})$ due to electron-phonon interaction within the usual Fröhlich model. To solve single impurity Anderson

problem we use NRG.[4] All calculations are done at nearly zero temperature and at half filling. For "bare" electrons we assume semielliptic DOS with half bandwidth D.

According to the Migdal theorem in adiabatic approximation[14] we can restrict ourselves with the simplest first-order contribution to $\Sigma_{ph}(\varepsilon,\mathbf{p})$, shown by diagram in Fig. 1. The main advantage of this is the possibility to neglect any order vertex corrections due to electron-phonon coupling which are small over adiabatic parameter $\frac{\omega_D}{\varepsilon_F} \ll 1$.[14] Contribution shown in Fig. 1 can be written as

$$\Sigma_{ph}(\varepsilon,\mathbf{p}) = ig^2 \sum_{\omega,\mathbf{k}} \frac{\omega_0^2(\mathbf{k})}{\omega^2 - \omega_0^2(\mathbf{k}) + i\delta} \frac{1}{\varepsilon + \omega + \mu - \varepsilon(\mathbf{p}+\mathbf{k}) - \Sigma(\varepsilon+\omega) - \Sigma_{ph}(\varepsilon+\omega,\mathbf{p}+\mathbf{k})}, \tag{3}$$

where g is the usual electron-phonon interaction constant and $\omega_0(\mathbf{k})$ is the phonon dispersion, which in our case is taken as in the standard Debye model

$$\omega_0(\mathbf{k}) = u|\mathbf{k}|, \quad |\mathbf{k}| < \frac{\omega_D}{u}. \tag{4}$$

Here u is the sound velocity and ω_D is Debye frequency. Actually $\Sigma_{ph}(\varepsilon,\mathbf{p})$ defined by Eq. (3) is momentum independent. Direct calculations (see, e.g., Ref. 15) for the case of Debye spectra [Eq. (4)] produce the lowest-order contribution to the self-energy [Eq. (3)] in the following form

$$\Sigma_{ph}(\varepsilon) = \frac{-ig^2}{4\omega_c^2} \int_{-\infty}^{+\infty} \frac{d\omega}{2\pi} \left\{ \omega_D^2 + \omega^2 ln \left| \frac{\omega_D^2 - \omega^2}{\omega^2} \right| + i\pi\omega^2 \theta(\omega_D^2 - \omega^2) \right\} I(\varepsilon+\omega) \tag{5}$$

with

$$I(\epsilon) = \int_{-D}^{+D} d\xi \frac{N_0(\xi)}{E_\varepsilon - \xi}, \tag{6}$$

where $E_\varepsilon = \varepsilon - \Sigma(\varepsilon) - \Sigma_{ph}(\varepsilon)$ and $\omega_c = p_F u$ is a characteristic frequency of the order of ω_D. For the case of semielliptic noninteracting DOS $N_0(\varepsilon)$ with half-bandwidth D we get

$$I(\epsilon) = \frac{2}{D^2}(E_\varepsilon - \sqrt{E_\varepsilon^2 - D^2}). \tag{7}$$

It is convenient to introduce the dimensionless electron-phonon coupling constant as[15]

FIG. 1. Migdal-type contribution to electron-phonon self-energy included in DMFT+Σ_{ph} scheme.

$$\lambda = g^2 N_0(\varepsilon_F) \frac{\omega_D^2}{4\omega_c^2}. \tag{8}$$

To simplify our analysis we shall not perform fully self-consistent calculations neglecting phonon renormalization due to EPI,[15] assuming that the phonon spectrum [Eq. (4)] is fixed by the experiment.

III. RESULTS AND DISCUSSION

Let us start from comparison between pure DMFT and DMFT+Σ_{ph} DOSs for strong ($U/2D=1.25$) and weak ($U/2D=0.625$) Hubbard interaction presented in Fig. 2 on upper and lower panels correspondingly. Dimensionless EPI constant [Eq. (8)] used in these calculations was $\lambda=0.8$ and Debye frequency $\omega_D=0.125$ D. In both cases we observe some spectral-weight redistribution due to EPI. For $U/2D=1.25$ (upper panel of Fig. 2) we see the well-developed three-peak structure typical for strongly correlated metals. In the energy interval $\pm\omega_D$ around the Fermi energy (which is taken as zero energy at all figures below) there is almost no difference in the DOS quasiparticle peak line shape obtained

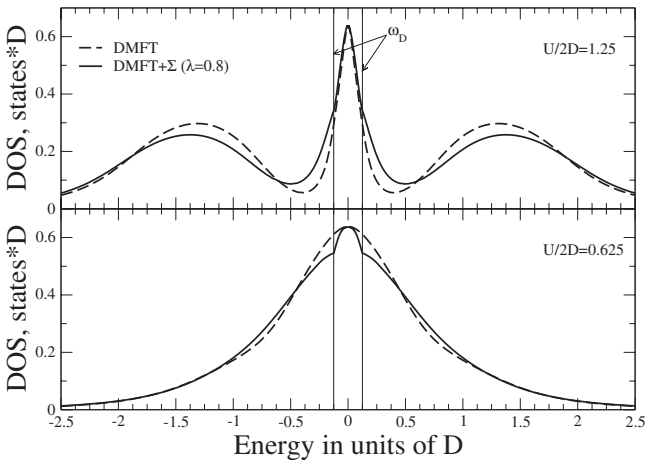

FIG. 2. Comparison of DOSs obtained within standard DMFT (dashed lines) and DMFT+Σ_{ph} (solid lines) methods for strong (upper panel, $U/2D=1.25$) and weak (lower panel, $U/2D=0.625$) Hubbard interaction regimes. Dimensionless electron-phonon coupling constant $\lambda=0.8$.

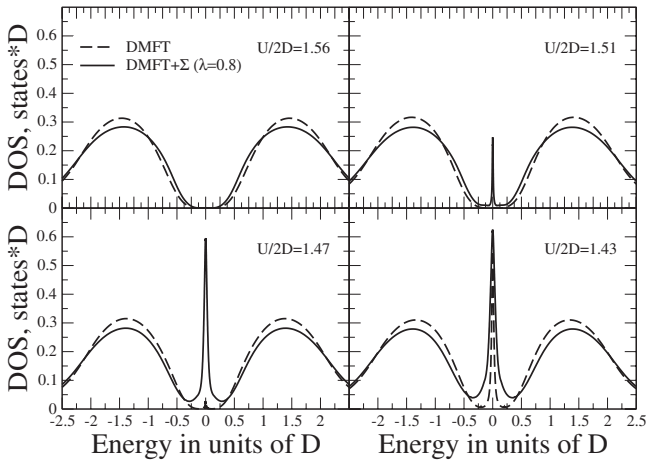

FIG. 3. Sequence of DOSs obtained within standard DMFT (dashed lines) and DMFT+Σ_{ph} (solid lines) methods close to metal-insulator transition (from top left to bottom right) with $\lambda=0.8$.

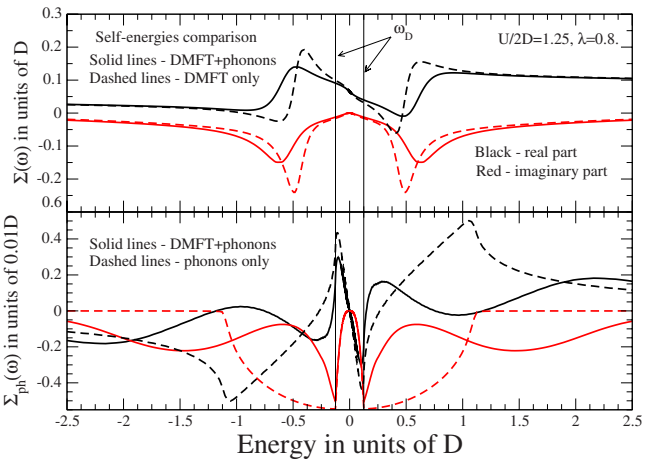

FIG. 4. (Color online) Upper panel—comparison of standard DMFT self-energies $\Sigma(\varepsilon)$ (dashed lines) with self-energies renormalized by phonons and obtained within the DMFT+Σ_{ph} approximation (solid lines). Lower panel—EPI self-energies $\Sigma_{ph}(\varepsilon)$. Black lines—real parts, gray (red) lines—imaginary parts. $\lambda=0.8$ and $U/2D=1.25$.

from pure DMFT and DMFT+Σ_{ph}. However outside this interval DMFT+Σ_{ph} quasiparticle peak becomes significantly broader with spectral weight coming from Hubbard bands. This broadening of DMFT+Σ_{ph} quasiparticle peak leads as we show below to inhibiting of metal to insulator transition. In the case of $U/2D=0.625$ there are no clear Hubbard bands formed but only some "side wings" are observed. Spectral-weight redistribution in the lower panel of Fig. 2 is not dramatic, though qualitatively different from the case of $U/2D=1.25$. Namely, main deviations between pure DMFT and DMFT+Σ_{ph} happen in the interval $\pm\omega_D$, where one can observe a kind of "cap" in DMFT+Σ_{ph} DOS. Corresponding spectral weight goes to the energies around $\pm U$, where Hubbard bands are supposed to form.

In Fig. 3 we compare the behavior of pure DMFT and DMFT+Σ_{ph} DOSs for different $U/2D$ values close to Mott-Hubbard metal-insulator transition. For $U/2D=1.56$ both standard DMFT and DMFT+Σ_{ph} produce insulating solution. However there is some difference between these solutions. The DMFT+Σ_{ph} Hubbard bands are lower and broader than DMFT ones because of additional interaction (EPI) included. With decrease in U for $U/2D=1.51$ and 1.47 we observe that DMFT+Σ_{ph} results correspond to metallic state (with narrow quasiparticle peak at the Fermi level) while conventional DMFT still produces insulating solution. Only around $U/2D=1.43$ both DMFT and DMFT+Σ_{ph} results turn out to be metallic. Overall DOSs lineshape is the same as discussed above. Thus with increase in U finite EPI slightly inhibits Mott-Hubbard transition from metallic to insulating phase. This result is similar to what was observed for the HHM in weak EPI regime.[16–18]

For more deep insight into these results let us analyze the structure of corresponding self-energies $\Sigma(\varepsilon)$ and $\Sigma_{ph}(\varepsilon)$. In Fig. 4 we show both real and imaginary parts of these self-energies. EPI changes $\Sigma(\varepsilon)$ rather significantly (see upper panel of Fig. 4). At the same time in $\pm\omega_D$ energy interval we find that slopes of real parts of both self-energies (which determines quasiparticle weight in the Fermi-liquid theory) are almost the same while imaginary parts are very close to zero. Thus quasiparticle peaks should be essentially identical in this region as we showed above (Fig. 2). At energies higher than Debye frequencies Re $\Sigma(\varepsilon)$ goes steeper with respect to Re$(\Sigma+\Sigma_{ph})$, making DMFT quasiparticle peak in DOS narrower above ω_D thus providing faster metal to insulator transition at $\lambda=0$. For the case of $U/2D=0.625$ (not shown here) pure DMFT self-energy and those with the account of EPI are nearly identical. Corresponding Σ_{ph} is very close to that obtained due to phonons only and shown in the lower panel of Fig. 4 with dashed lines. It produces only the cap in the DOS around the Fermi level mentioned above. One can say also that such a cap appears in DOS when energy interval $2\omega_D$ is much smaller than the quasiparticle peak width.

Now we address the issue of a sudden change in the slope of electronic dispersion, the so-called kinks. It is well known that interaction of electrons with some bosonic mode produces such a kink. In the case of EPI typical kink energy is just the Debye frequency ω_D. Kinks of purely electronic nature were recently reported in Ref. 10.

The energy of purely electronic kink as derived in Ref. 10 for semielliptic bare DOS is given by

$$\omega^* = Z_{FL}(\sqrt{2}-1)D, \tag{9}$$

where D is the half of bare bandwidth and $Z_{FL}=(1-\frac{\partial \mathrm{Re}\,\Sigma)}{\partial\varepsilon}\big|_{\varepsilon=\varepsilon_F})^{-1}$ is Fermi-liquid quasiparticle weight. The rough estimate of ω^* is given by the half width of quasiparticle peak of DOS at its half height. Schematic pictures of kinks of both kinds close to the Fermi level are shown in Fig. 5. Electronic kink (on the right side) is rather "round" and usually hard to see. This kink is formed by the smaller slope connection of two split branches with initial slope (dashed line) at energy $\pm\omega^*$. Far away from the Fermi level both of these branches return to the initial dispersion. In contrast the phonon kink produces rather sharp deviation from the initial dispersion at ω_D but outside $\pm\omega_D$ energy interval electron dispersion quickly returns to the initial one.

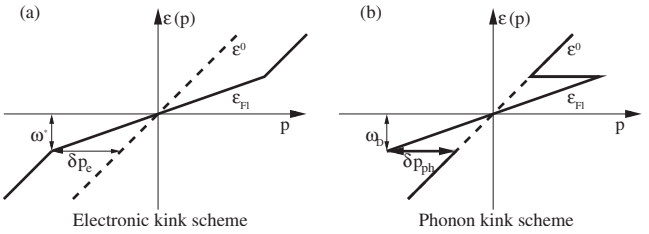

FIG. 5. Schematic picture of pure electronic kink [panel (a)] and phonon kink [panel (b)] in electron energy dispersion near the Fermi level. ε^0—bare energy dispersion with no interactions included; ε_{Fl}—dispersion around the Fermi level with electron interaction included; ω^*—electronic kink energy; ω_D—phonon kink (Debye) energy; δp_e and δp_{ph}—shifts of dispersion due to pure electronic and phonon kinks.

Our calculations clearly demonstrate that electronic kinks are hardly observable on the background of phonon kinks (as, e.g., in upper panel of Fig. 4) and special care should be taken to separate them by rather fine tuning of the parameters of our model. To clarify this situation we introduce an additional characteristic of the kink—the shift of electron dispersion in momentum space δp at kink energy. From simple geometry we estimate for phonon kinks

$$\delta p_{ph} = \frac{\omega_D}{v_F}\lambda, \tag{10}$$

where v_F is the bare Fermi velocity and λ was defined in Eq. (8). For electronic kink the similar estimate is

$$\delta p_e = \frac{\omega^*}{v_F^*}\left(1 - \frac{Z_{FL}}{Z_0}\right) \equiv \frac{\omega^*}{v_F^*}\lambda_e, \tag{11}$$

where Z_0 is quasiparticle weight in the case of absence of electronic kinks (the same as Z_{cp} defined in Ref. 10). Velocity v_F^* is the Fermi velocity of initial dispersion but it cannot be just a bare one. As was reported in Ref. 10 electronic kinks can be observed only for rather strong Hubbard interaction when three-peak structure in the DOS is well developed and electronic dispersion is strongly renormalized by correlation effects. This renormalization is determined by λ_e defined in Eq. (10), which can be seen as kind of dimensionless interaction constant. In the case when both slopes on the Fermi level and out of $\pm\omega^*$ energy interval are equal there will be no electronic kink at all.

Now we can choose parameters of our model to make both kinks simultaneously visible. First of all one should take care that $\omega_D \ll \omega^*$. For $U/2D=1$ with $U=3.5$ eV we get $\omega^* \sim 0.1$ D and a reasonable value of Debye frequency is $\omega_D \sim 0.01$ D. To make phonon kink pronounced at such relatively low Debye frequency [cf. Eq. (10)] we have to increase EPI constant. So we take $\lambda=2.0$. Corresponding quasiparticle peaks of the DOS together with $\mathrm{Re}(\Sigma+\Sigma_{ph})$ are shown in Fig. 6: in the left panel EPI is switched off while in the right panel it is switched on. We can see that $2\omega^*$ is approximately width of the quasiparticle peak of well-developed three-peak structure (see upper panel of Fig. 2) and energy position of electronic kinks are marked by arrows. On the right side of Fig. 6, where EPI is present, phonon kinks at $\pm\omega_D$ are clearly visible and well separated in energy from electronic kink position.

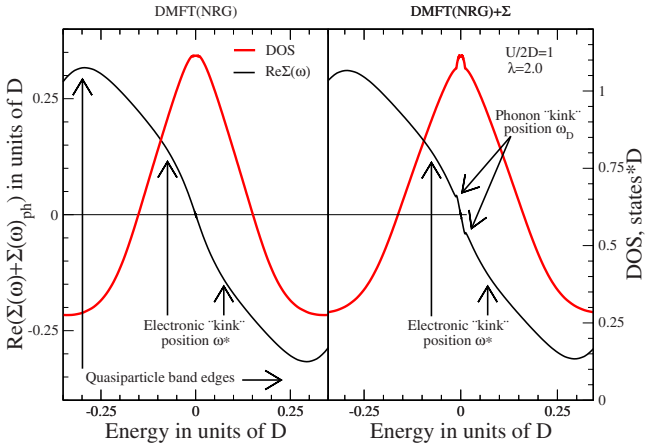

FIG. 6. (Color online) Quasiparticle part of DOSs (see Fig. 2, upper panel) (red line) and corresponding real part of additive self-energy $\mathrm{Re}(\Sigma+\Sigma_{ph})$ with electron-phonon coupling switched off (left panel) and switched on (right panel). $\lambda=2.0$ and $U/2D=1$.

To demonstrate coexistence of both these types of kinks we take a look at energy dispersion of simple cubic lattice with nearest-neighbor's transfers only. Most convenient is high-symmetry $\Gamma-(\pi,\pi,\pi)$ direction.[10] In Fig. 7 dispersion along this direction around Fermi level is shown. Black line with diamonds is pure DMFT electronic spectrum while gray (red) line with circles represents the result of DFMT+Σ_{ph} calculations. Electronic and phonon kinks are marked with arrows.

Finally we address the behavior of phonon kinks in electronic spectrum as a function of Hubbard interaction U. As $U/2D$ ratio grows Fermi velocity in Eq. (10) goes down so that momentum shift of kink position δp moves away from p_F while kink energy remains at ω_D. This is confirmed by our direct DMFT+Σ_{ph} calculations producing the overall picture of spectrum evolution shown in Fig. 8.

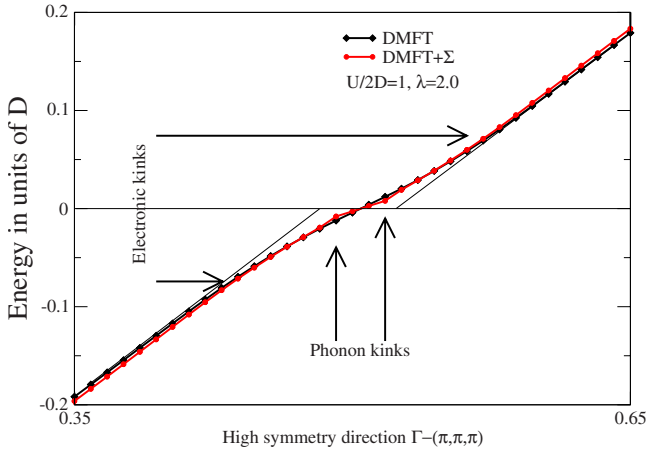

FIG. 7. (Color online) Quasiparticle dispersions obtained from standard DMFT (black lines with diamonds) and DMFT+Σ_{ph} (red lines with circles) around the Fermi level and along the part of high-symmetry direction $\Gamma-(\pi,\pi,\pi)$.

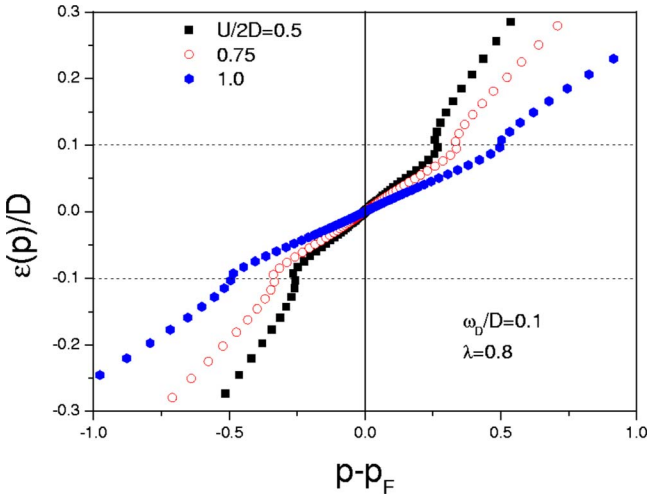

FIG. 8. (Color online) Quasiparticle dispersions around Fermi level with phonon kinks obtained from DMFT+Σ_{ph} calculations for different interaction strengths $U/2D=0.5$, 0.75, and 1.0; $\lambda=0.8$ and $\omega_D=0.1$ D.

IV. CONCLUSION

This work analyzes strongly correlated electrons, treated within DMFT approach to the Hubbard model, interacting with Debye phonons. EPI is treated within the adiabatic approximation (Migdal theorem), allowing the neglect of vertex corrections for $\lambda < \frac{e_F}{\omega_D} \sim 10$.[15] However some authors expressed different point of view that due to polaronic effects, applicability of Migdal theorem is restricted to $\lambda < 1$.[19] DMFT+Σ_{ph} approach allows us to use the standard momentum space representation for phonon self-energy [Eq. (3)] while the general structure of DMFT equations remains intact.

Mild EPI leads to rather insignificant changes in electron density of states, both in correlated metal and in Mott-insulator state, slightly inhibiting metal to insulator transition with increase in U. However, kinks in the electronic dispersion due to EPI dominate for the most typical values of the model parameters, making kinks of purely electronic nature, predicted in Ref. 10, hardly observable. Special care (fine tuning) of model parameters is needed to separate these anomalies in electronic dispersion in strongly correlated systems.

We have also studied phonon kinks evolution with the strength of electronic correlations demonstrating the significant drop in the slope of electronic dispersion close to the Fermi level with the growth of Hubbard interaction U. We believe that these results may be of importance in further studies of the evolution of electronic spectra in highly correlated systems, such as copper oxides.

ACKNOWLEDGMENTS

We are grateful to Th. Pruschke for providing us with his effective NRG code. This work is partly supported by RFBR under Grants No. 08-02-00021, No. 08-02-91200, and No. 08-02-00712. It was performed within the framework of the programs of fundamental research of the Russian Academy of Sciences (RAS) "Quantum physics of condensed matter" and of the Physics Division of RAS "Strongly correlated electrons in solid states." I.N. acknowledges the Russian Science Support Foundation and Grant of President of Russia MK-614.2009.2.

[1] J. Hubbard, Proc. R. Soc. London, Ser. A **276**, 238 (1963); **277**, 237 (1964); **281**, 401 (1964); **285**, 542 (1965); **296**, 82 (1967); **296**, 100 (1967).
[2] T. Holstein, Ann. Phys. (N.Y.) **8**, 325 (1959).
[3] A. Georges, G. Kotliar, W. Krauth, and M. J. Rozenberg, Rev. Mod. Phys. **68**, 13 (1996).
[4] R. Bulla, T. A. Costi, and T. Pruschke, Rev. Mod. Phys. **80**, 395 (2008).
[5] A. C. Hewson and D. Mayer, J. Phys.: Condens. Matter **14**, 427 (2002).
[6] A. Lanzara, P. V. Bogdanov, X. J. Zhou, S. A. Kellar, D. L. Feng, E. D. Lu, T. Yoshida, H. Eisaki, A. Fujimori, K. Kishio, J.-I. Shimoyama, T. Noda, S. Uchida, Z. Hussain, and Z.-X. Shen, Nature (London) **412**, 510 (2001).
[7] Z.-X. Shen, A. Lanzara, S. Isihara, and N. Nagaosa, Philos. Mag. B **82**, 1349 (2002).
[8] J. P. Hague, J. Phys.: Condens. Matter **15**, 2535 (2003).
[9] W. Koller, A. C. Hewson, and D. M. Edwards, Phys. Rev. Lett. **95**, 256401 (2005).
[10] K. Byczuk, M. Killar, K. Held, Y.-F. Yang, I. A. Nekrasov, Th. Pruschke, and D. Vollhardt, Nat. Phys. **3**, 168 (2007).
[11] E. Z. Kuchinskii, I. A. Nekrasov, and M. V. Sadovskii, JETP Lett. **82**, 198 (2005).
[12] M. V. Sadovskii, I. A. Nekrasov, E. Z. Kuchinskii, Th. Pruschke, and V. I. Anisimov, Phys. Rev. B **72**, 155105 (2005).
[13] E. Z. Kuchinskii, I. A. Nekrasov, and M. V. Sadovskii, Phys. Rev. B **75**, 115102 (2007).
[14] A. D. Migdal, Zh. Eksp. Teor. Fiz. **34**, 1438 (1958) [Sov. Phys. JETP **7**, 999 (1958)].
[15] M. V. Sadovskii, *Diagrammatics* (World Scientific, Singapore, 2006), pp. 75–76.
[16] W. Koller, D. Mayer, Y. Õno, and A. C. Hewson, Europhys. Lett. **66**, 559 (2004).
[17] G. S. Jeon, T.-H. Park, J. H. Han, H. C. Lee, and H.-Y. Choi, Phys. Rev. B **70**, 125114 (2004).
[18] W. Koller, D. Meyer, and A. C. Hewson, Phys. Rev. B **70**, 155103 (2004).
[19] A. S. Aleksandrov and E. A. Mazur, Zh. Eksp. Teor. Fiz. **96**, 1773 (1989).